

Figure 4: Crack spacing representation using TCM

where d_b is the diameter of the reinforcing bar, τ_b is a bond-stress parameter, usually taken as $\tau_b = 2f_{ct}$ for short term loading scenarios (Marti et al. 1998) and ρ_{tc} is the reinforcing ratio (A_{st}/A_{ct}). Similarly, the stress in the steel between two primary cracks depends on τ_b and d_b . At any point adjacent to the primary crack, the stress in the steel may be taken as:

$$\sigma_s(x) = \frac{T_s}{A_{st}} - \frac{4\tau_b x}{d_b} \dots 0 \leq x \leq s_r/2 \quad (2)$$

where A_{st} is the cross-sectional area of steel, and T_s is the force in the steel reinforcing bar. Setting Equation 2 to f_{ct} at $x = s_r/2$ yields an expression for the maximum spacing, between two primary cracks:

$$s_{max} = \frac{(f_{ct} - \sigma_f(w))d_b}{2\tau_b\rho_{tc}} \quad (3)$$

By the TCM, the minimum crack spacing is half the maximum value, that is $s_{min} = s_{max}/2$. The median crack spacing is taken as λs_{max} , where $\lambda \in [0.5, 1]$. This is the same expression as derived by Pfyl (2003). Examining Figure 4 and Equation 3, it is clear that the inclusion of fibres, as a means of transmitting stress across a crack in concrete, reduces the crack spacing. This is a function of the maximum stress that can be carried after cracking and the initial crack width before the crack pattern has stabilized.

Now let us consider the average stress carried through a SFRC tension tie. For the maximum crack spacing scenario presented in Figure 3a, the average stress carried by the fibres and concrete is equivalent to:

$$\sigma_{C,avg,max} = 0.5f_{ct} \left(1 + \sigma_f(w)/f_{ct}\right) \quad (4)$$

where $\sigma_f(w)$ is the residual tensile stress carried by the SFRC at a crack opening displacement (COD), w . The average stress carried by the fibres and concrete along the tension chord for the minimum crack spacing scenario (Figure 3b) is equivalent to:

$$\sigma_{C,avg,min} = 0.25f_{ct} \left(1 + 3\sigma_f(w)/f_{ct}\right) \quad (5)$$

Amin et al. (2016) equated the median tension stiffening along the length of a given SFRC tension chord with many cracks by considering the average stress carried by the two scenarios above giving:

$$\sigma_{C,avg} = 0.125f_{ct} \left(3 + 5\sigma_f(w)/f_{ct}\right) \quad (6)$$

Amin (2015) extensively verified the TCM for many SFRC tension ties tested by a number of researchers (Deluce, 2011; Minelli et al 2015) and good correlation was shown against the experimental data when $\sigma_f(w)$ was taken as $f_{0.5}$ in Equations 3 and 6.

3 Simplified instantaneous deflection calculation

Consider a SFRC concrete beam of rectangular cross section after cracking. The beam can be idealized as a compression chord of depth d_n and width b and a cracked tension chord consisting of the tensile steel reinforcement A_{st} surrounded by an area of tensile concrete, A_{ct} (see Figure 5), with A_{ct} usually taken as one third of the area below the neutral axis. The short term, instantaneous deflection of a SFRC one-way member subjected to bending can be readily determined once the tension stiffening relationship of the element is established. Often, modelling the tension stiffening effect in deflection calculations for reinforced concrete members involves determining an average effective second moment of area (I_e) for a cracked member, where the effective second moment of area is empirically interpolated between the second moment of areas of the uncracked section (I_g) and the fully cracked section (I_{cr}). Deflections can then be determined by double integration of the curvatures $\chi = M/E_c I_e$ along the length of the member.

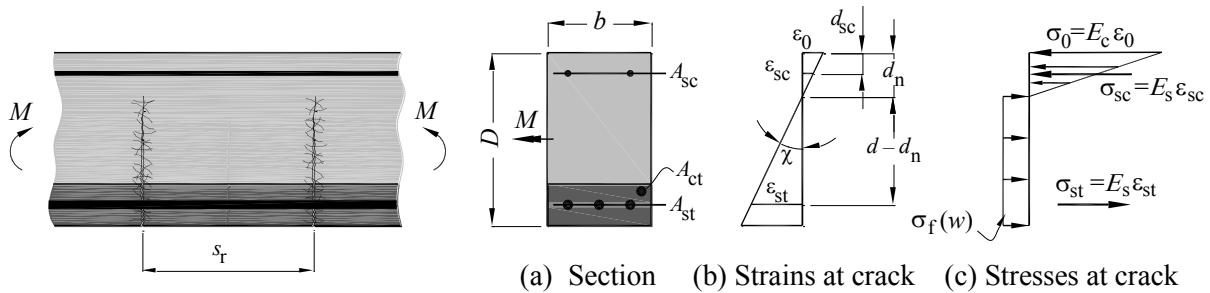


Figure 5: Strains and stresses on a cracked SFRC rectangular section in flexure

Another method was developed by Kenel (2002) who extended the TCM and established moment-curvature relationships for different loading scenarios of reinforced concrete beams. Amin et al. (2017) adapted this model to include the beneficial effects of the fibres to the moment-curvature relationship of reinforced concrete through tension stiffening. The deflection at mid-span of a member cracked in bending may be taken as:

$$\delta = \delta_{cr} - \Delta\delta_1 \quad (7)$$

where δ_{cr} is the deflection of the member that would be obtained assuming the section is fully cracked over the entire length of the member and the term $\Delta\delta_1$ accounts for the tension stiffening effect of the cracked fibre reinforced concrete. Expressions for δ_{cr} , and $\Delta\delta_1$, are presented in Table 1 and their physical representation is illustrated in Figure 6. In Table 1, $I_g = bD^3/12$ and $M_{cr} = f_{ct}bD^2/6$ are suitable approximations for a rectangular section.

The term $\Delta\chi$ in Table 1 represents the tension stiffening component of curvature due to the cracked fibre-concrete. To account for the beneficial effects to tension stiffening of the fibres crossing the cracks in SFRC members, Amin et al. (2017) derived $\Delta\chi$ as:

$$\Delta\chi = [(0.75 + 1.25f_{0.5}/f_{ct})bf_{ct}]/(6A_{st}E_s) \quad (8)$$

To simplify the computational effort required in deriving an expression for I_{cr} for SFRC, a reasonable approximation for $I_{cr,SFRC}$ may be taken as 1.1 $I_{cr,RC}$, where $I_{cr,RC}$ is the 2nd moment of area for a non-fibre reinforced concrete section and can be evaluated from elastic analysis. For rectangular sections, $I_{cr,RC}$ is:

$$I_{cr,RC} = \frac{bd_{n,RC}^3}{3} + nA_{st}(d - d_{n,RC})^2 + (n-1)A_{sc}(d_{n,RC} - d_{sc})^2 \quad (9a)$$

$$d_{n,RC} = d \left(\sqrt{\left(n\rho + (n-1)\rho' \right)^2 + 2n\rho + \frac{2(n-1)d_{sc}\rho'}{d}} - n\rho - (n-1)\rho' \right) \quad (9b)$$

where $\rho = A_{st}/(bd)$, $\rho' = A_{sc}/(bd)$, n is the modular ratio E_s/E_c , and d is the effective depth of the section. Similarly, the depth to the neutral axis in a SFRC section may be approximated as $d_{n,SFRC} = 1.2 d_{n,RC}$. Note that for lightly longitudinally reinforced members, the proposed simplifications may be overly conservative.

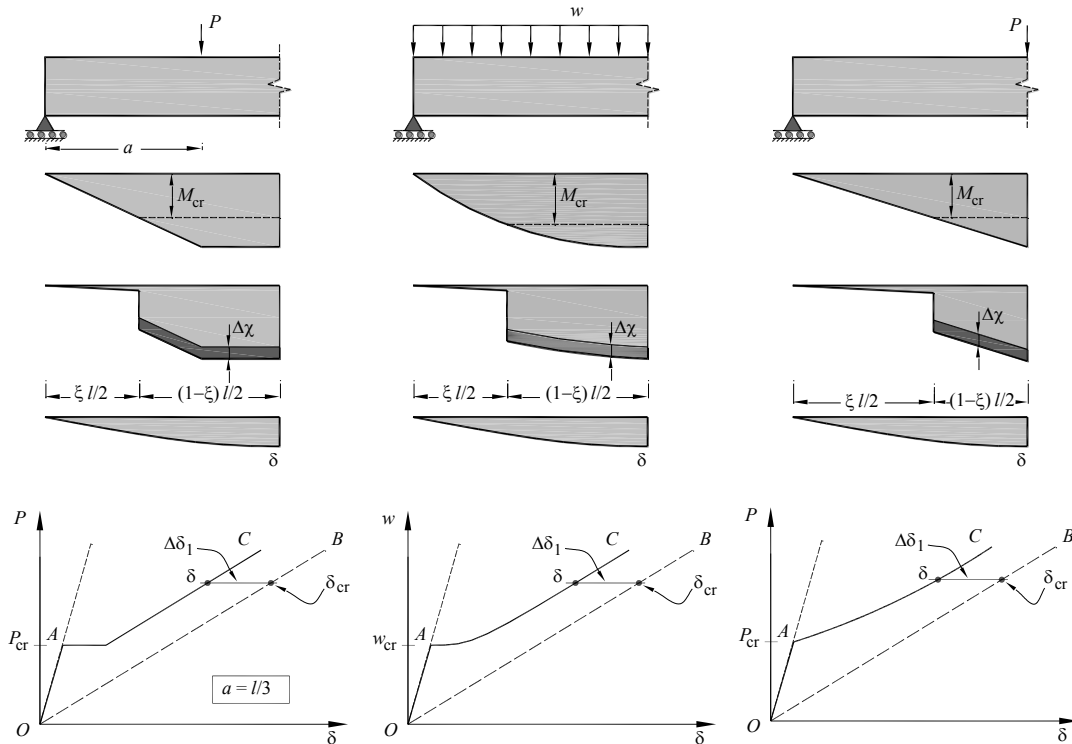


Figure 6: Beam notations, bending moments, curvatures and definitions of δ_{cr} and $\Delta\delta_1$

Table 1: Definitions of δ_{cr} and $\Delta\delta_1$ (see Kenel 2002, Amin et al. 2017)

| | δ_{cr} | $\Delta\delta_1$ | ξ |
|-----------------------|--|---|---------------------------------------|
| Four Point Bending | $\frac{Pl^2 a}{24E_c J_{cr,SFRC}} \left(3 - \frac{4a^2}{l^2} \right)$ | $\Delta\chi \left(1 - \xi^2 \right) \frac{l^2}{8}$ | $\frac{4M_{cr}}{Pl}$ |
| Uniformly Distributed | $\frac{5wl^4}{384E_c J_{cr,SFRC}}$ | $\Delta\chi \left(1 - \xi^2 \right) \frac{l^2}{8}$ | $1 - \sqrt{1 - \frac{8M_{cr}}{wl^2}}$ |
| Three Point Bending | $\frac{Pl^3}{48E_c J_{cr,SFRC}}$ | $\Delta\chi \left(1 - \xi^2 \right) \frac{l^2}{8}$ | $\frac{4M_{cr}}{Pl}$ |

4 Simplified instantaneous crack width calculation

For plain reinforced concrete tension ties, Gilbert (2008) determined an expression for the instantaneous crack width of a primary crack, w_i , in a reinforced concrete tension tie as being the difference between the elongation of the tensile steel between two primary cracks and the elongation of the concrete between the cracks. Following the notation introduced above, Gilbert's Equation for instantaneous cracks widths in plain reinforced concrete tension ties is written as:

$$w_i = \Delta_s - \Delta_c \quad (10a)$$

$$\Delta_s = \frac{2}{E_s} \int_0^{s_r/2} \left(\frac{T_s}{A_{st}} - \frac{4\tau_b x}{d_b} \right) dx = \frac{T_s s_r}{E_s A_{st}} - \frac{s_r^2 \tau_b}{E_s d_b} \quad (10b)$$

$$\Delta_c = \frac{2}{E_c} \int_0^{s_r/2} \left(\frac{4\tau_b \rho_{tc} x}{d_b} \right) dx = \frac{s_r^2 \tau_b \rho_{tc}}{E_c d_b} \quad (10c)$$

where T_s is the force in the longitudinal steel reinforcing bar (and equal to $T = M/z$ for members not containing fibres), E_s and E_c are the elastic moduli of the steel and concrete, respectively, and z is the internal lever arm between the tensile reinforcement and the resultant compressive force on the cracked section. To incorporate the stress carried by the fibres at the crack, Amin and Gilbert (2018) expressed Equation 10c as:

$$\Delta_c = \frac{2}{E_c} \int_0^{s_r/2} \left(\frac{4\tau_b \rho_{tc} x}{d_b} + \sigma_f(w) \right) dx = \frac{s_r^2 \tau_b \rho_{tc}}{E_c d_b} + \frac{s_r \sigma_f(w)}{E_c} \quad (11)$$

A close look at Equations 10a & 11 show that the crack width w_i is not an explicit equation of the independent variables since the stress carried by the fibres at a crack $\sigma_f(w)$ is itself a function of the crack width. Calculation of w_i therefore requires iteration. A detailed description of this process pertaining to SFRC beams can be found in Amin and Gilbert (2018). A conservative closed form solution to Equation 10 may be obtained by noting that Equation 11 approaches 0 as the applied moment increases to that which induces yielding to the longitudinal reinforcing steel. From an elastic analysis of a cracked cross-section subjected to a moment M_a greater than the instantaneous cracking moment M_{cr} , T_s may be approximated as:

$$T_s = \frac{nM_a (d - d_{n,SFRC})}{I_{cr,SFRC}} A_{st} \quad (12)$$

where M_a is the applied moment on the section. Expanding Equation 10a we may express the instantaneous crack width for a SFRC beam as:

$$w_i = \frac{s_r}{E_s} \left[\frac{nM_a (d - d_{n,SFRC})}{I_{cr,SFRC}} - \frac{s_r \tau_b}{d_b} \right] \quad (13)$$

Further research is required to accurately quantify any time-dependent changes of crack widths and deformations (i.e. due to the effects of compressive creep of the uncracked concrete in the compressive zone, tensile creep of concrete in the cracked part of the cross-section, bond creep between the reinforcement/fibres and the concrete, and shrinkage).

5 Example

5.1 Specimen geometry and material properties

Consider a uniformly loaded simply-supported SFRC beam of rectangular cross section, with width, $b = 300$ mm, overall depth, $D = 500$ mm and the span is 5 m. The beam is reinforced longitudinally with two 20 mm diameter bars at the top of the section (at a depth to the centre of the bars $d_{sc} = 50$ mm) and three 24 mm diameter bars at the bottom. The effective depth to the centroid of the bottom tensile bars $d = 450$ mm. The design strength of all reinforcing steels is 500 MPa. The beam is subjected to a short term factored loading equivalent to $w_s = 35$ kN/m resulting in an applied in service moment of 109.4 kNm. The beam is reinforced with 30 kg/m³ (0.38%) Dramix[®] RC-65/35-BN cold drawn wire fibers. The characteristic compressive strength of the concrete is $f'_c = 40$ MPa, the characteristic uniaxial tensile strength is $f'_{ct} = 3.05$ MPa, the characteristic residual tension at a crack width of 0.5 mm is $f_{0.5} = 0.63$ MPa and the elastic modulus (E_c) of the concrete is 33.5 GPa.

5.2 Instantaneous deflection

The depth to the neutral axis is first evaluated assuming no contribution provided by the fibres. In this case, the tensile and compressive reinforcement ratios are: $\rho = 1350/(300 \times 450) = 0.0100$, $\rho' = 620/(300 \times 450) = 0.0046$ and the modular ratio, $n = 200/33.5 = 5.97$. Substituting these values into Equation 9b and 9b gives $d_{n,RC} = 125.9$ mm and $I_{cr,RC} = 1063.9 \times 10^6$ mm⁴. Approximating the second moment of area for the SFRC beam as $1.1I_{cr,RC}$ gives $I_{cr,SFRC} = 1170.3 \times 10^6$ mm⁴. From Table 1:

$$\delta_{cr} = \frac{5wl^4}{384E_c I_{cr,SFRC}} = \frac{5 \times 35 \times 5000^4}{384 \times 33500 \times 1170 \times 10^6} = 7.27 \text{ mm}$$

and the stiffening component provided by the cracked fibre reinforced concrete is

$$\Delta\delta_1 = \Delta\chi(1 - \xi^2)l^2/8$$

where $\Delta\chi$ is given by Equation 8 and ξ is obtained from Table 1.

The cracking moment is evaluated as $M_{cr} = f'_{ct}bD^2/6 = 3.05 \times 300 \times 500^2/6 = 38.13$ kNm. Solving yields $\Delta\delta_1 = 1.71$ mm and hence, the deflection of the beam under this applied load is equal to $\delta = \delta_{cr} - \Delta\delta_1 = 5.56$ mm.

5.3 Instantaneous crack width

The instantaneous crack width, w_i , of the section is a function of the crack spacing, s_r and the applied moment. The crack spacing is defined in Equation 3 and is a function of the effective reinforcing ratio ($\rho_{tc} = A_{st}/A_{ct}$) of the assumed tension tie, the bond strength between the fibre-concrete and reinforcing bar and $f'_{0.5}$. Assuming $\tau_b = 2 f'_{ct}$ and A_{ct} is one third of the area below the neutral axis (and noting $d_{n,SFRC} \approx 1.2 d_{n,RC}$) gives:

$$\rho_{tc} = \frac{1350}{1/3 \times (500 - 1.2 \times 125.9) \times 300} = 0.0387$$

and hence the crack spacing (Equation 3) and the instantaneous crack width (Equation 13) are:

$$s_r = \frac{(3.05 - 0.63) \times 24}{2 \times 2 \times 3.05 \times 0.0387} = 123 \text{ mm} \quad \text{and}$$

$$w_i = \frac{123}{200000} \left[\frac{5.97 \times 109.4 \times 10^6 (450 - 1.2 \times 125.9)}{1170 \times 10^6} - \frac{123 \times 2 \times 3.05}{24} \right] = 0.08 \text{ mm}$$

Using the method above for the same member not containing any fibres (i.e. with $f'_{0.5} = 0$ MPa) results in $\delta = 6.72$ mm, $s_r = 155$ mm, $w_i = 0.12$ mm.

6 Concluding remarks

In this paper, rationale expressions suitable for design are presented to describe the in-service behaviour of SFRC beams. Following a description of the tension stiffening effect in SFRC members co-reinforced with conventional steel reinforcement a short design example is provided to highlight the benefits of utilising SFRC in reducing instantaneous deflections, crack widths and crack spacing.

7 References

- Amin, A. 2015. Post cracking behavior of steel fiber reinforced concrete: from material to structure. *PhD Dissertation*. UNSW Australia.
- Amin, A., and Gilbert, R.I. 2018. Instantaneous crack width calculation for steel fiber reinforced concrete flexural members. *ACI Structural Journal* 115(2): 535-544.
- Amin, A., Foster, S.J., and Kaufmann, W. 2017. Instantaneous deflection calculation for steel fiber reinforced concrete one way members. *Engineering Structures* 131: 438-445.
- Amin, A., Foster, S.J., and Muttoni, A. 2015. Derivation of the σ - w relationship for SFRC from prism bending tests. *Structural Concrete*, 16 (1): 93-105.
- Amin, A., Foster, S.J., and Watts, M. 2016. Modelling the tension stiffening effect in steel fiber reinforced-reinforced concrete. *Magazine of Concrete Research* 68 (7): 339-352.
- Deluce, J. 2011. Cracking behavior of steel fibre reinforced concrete containing conventional steel reinforcement. *MASc Dissertation*. The University of Toronto.
- AS5100.5. 2017. Australian Standard, bridge design part 5: concrete. Standards Australia.
- EN 14651. 2007. Test method for metallic fibre concrete- measuring the flexural tensile strength (LOP, residual). European Committee for Standardization: 17 pp.
- fib Model Code 2010. 2013. *Model Code 2010*. Fédération Internationale du Béton: 402 pp.
- Gilbert, R.I. 2008. Control of flexural cracking in reinforced concrete. *ACI Structural Journal* 105(3): 301-307.
- Kenel, A. 2002. Biegetragverhalten und Mindestbewehrung von Stahlbetonbauteilen. *PhD Dissertation*, No.14874. Swiss Federal Institute of Technology, Switzerland. (in German).
- Marti, P., Alvarez, M., Kaufmann, W., and Sigrist, V. 1998. Tension chord model for structural concrete. *Structural Engineering International* 8(4): 287-298.
- Minelli, F and Plizzari, G. 2015. Derivation of a simplified stress-crack width law for Fiber Reinforced Concrete through a revised round panel test. *Cement and Concrete Composites*, 58: 95-104.
- Pfyll, T. 2003. Tragverhalten von Stahlfaserbeton. *PhD Dissertation, IBK-Report No.279*. Swiss Federal Institute of Technology, Switzerland. (in German).

The effect of fibres on corrosion of reinforced concrete

Carlos G. Berrocal^{1,2}, Karin Lundgren¹, Ingemar Löfgren^{1,2}

¹ : Department of Architecture and Civil Engineering, Division of Structural Engineering, Chalmers University of Technology, Gothenburg, Sweden.

² : Thomas Concrete Group, Gothenburg, Sweden.

Abstract

In the present paper, long-term experiments involving natural corrosion of RC beams subjected to chloride solution cyclic exposure were carried out to investigate the effect of fibres on different aspects of the corrosion process as well as their contribution to the structural behaviour of RC elements damaged by corrosion. The long-term experiments were complemented with short-term accelerated corrosion experiments and mechanical tests to investigate the influence that low fibre contents may have on individual mechanisms that play an important role in the corrosion process of steel in concrete. These showed that fibres promote crack branching which results in a change of the internal crack pattern towards multiple thinner cracks, particularly near the reinforcement. This agrees with the long-term experiment results, which exhibited longer times to corrosion initiation for FRC beams with bending cracks and revealed a more distributed corrosion with more pits but less cross-sectional loss compared to bars in plain concrete. Fibres also proved beneficial in delaying corrosion-induced cracks and preventing cover spalling, which greatly enhanced the bond-behaviour of corroded bars. Furthermore, a positive effect of the fibres was also observed on the residual flexural capacity of corroded beams, which generally increased the load-carrying capacity and rotation capacity.

Keywords

Chloride-induced corrosion, durability, cracking, reinforcement bond, residual flexural capacity

1 Introduction

The mechanical and fracture properties of FRC have been extensively investigated for several decades. As a result, fibres are currently used in various applications such as industrial floors or slabs on grade to control shrinkage cracks as well as in tunnels as sprayed concrete or segmental linings. Moreover, the incorporation of design rules for FRC in recently released standards and codes, see e.g. (Model Code, 2010; Swedish Standards Institute, 2014), shows the increasing interest in using FRC in a broader range of structural applications. However, due to the casting-dependent distribution and orientation of the fibres throughout the concrete matrix, fibre reinforcement may, in many cases, be only used in combination with conventional reinforcement bars. Available research has shown that incorporating fibres into RC elements results in an improved mechanical performance with regards to increased load capacity and tension-stiffening as well as enhanced bond-behaviour. Nevertheless, one of the main advantages of FRC is the improved crack control mechanisms provided by crack-bridging fibres.

Cracks in RC elements are often regarded as preferential paths for the ingress of detrimental agents, such as CO₂ and chloride ions, that eventually result in the initiation of reinforcement corrosion. Moreover, numerous observations indicate that wider cracks shorten the time-to-corrosion initiation (Schiessl & Raupach, 1997; Tuutti, 1982), which has led current structural codes, see e.g. (ACI Committee 318, 2011; EN 1992-1-1 Eurocode 2, 2004), to prescribe strict crack width limitations as a way to mitigate the deterioration of RC structures due to corrosion of reinforcement. Consequently, combining fibres and conventional reinforcement to obtain narrower and more closely spaced cracks could be beneficial to delay the initiation of reinforcement corrosion, as shown in various investigations (Berrocal, Löfgren, Lundgren, & Tang, 2015; Sappakittipakorn & Banthia, 2012). Furthermore, several researchers have reported that steel fibres possess an enhanced corrosion resistance compared to traditional reinforcement bars (Dauberschmidt, 2006; Mangat & Gurusamy, 1988; Marcos-Meson et al., 2018). On the other hand, studies addressing the potential impact of fibres on the corrosion process of conventional reinforcement are very sparse (Grubb, Blunt, Ostertag, & Devine, 2007; Kim, Boyd, & Lee, 2010; Shaikh, Mihashi, & Kobayakawa, 2015) and have mainly focused on experimental results from uncracked specimens subjected to artificial corrosion through impressed current. Similarly, studies investigating the effect of fibres on the structural behaviour of RC elements with corroding reinforcement are even scarcer (Blunt, Jen, & Ostertag, 2015; Maalej, Ahmed, & Paramasivam, 2003), and have been mainly directed towards the study of cementitious composites with high fibre dosages exhibiting strain hardening behaviour.

To achieve a generalized deployment of FRC into a broader range of structures, including those susceptible to suffer corrosion damage, a sound understanding of how the fibres may influence the corrosion process of conventional rebars and the structural behaviour of corroded RC elements is required. The present paper summarizes the results from a PhD project aimed at investigating the effect of low fibres contents (<1% vol.) on different aspects of the corrosion process. These aspects include how the fibres, through a change of the internal crack morphology, may influence the ingress of detrimental agents into the concrete as well as the initiation and propagation phases of reinforcement corrosion. Moreover, the contribution of the fibres to the structural behaviour of RC elements damaged by corrosion has been also investigated through pullout and flexural tests.

2 Experimental programme

The experimental programme presented in this work is comprised of three different studies, the main study consisting of long-term experiments, referred to as experimental study A, and two short-term complementary experiments, referred to as experimental study B and C, respectively. Experimental study A was intended to encompass the different stages of the corrosion process while reproducing, as much as possible, realistic conditions. These conditions included the combination of naturally induced accelerated corrosion, flexural cracks formed under mechanical loading, varying crack widths and different loading conditions. The short-term experiments, on the other hand, were designed to isolate the effect of fibres on specific parameters relevant to the corrosion process, namely the effect on the internal crack morphology and the bond behaviour between concrete and corroding reinforcement. In the following, a brief description of each experimental study is provided.

2.1 Experimental study A: long-term corrosion experiments

A total of 54 beam specimens were cast. Six of these were kept uncracked and stored in potable water to be used as reference samples, while the remaining were subjected to different loading conditions and subsequently exposed to chlorides. The four conditions considered were:

- (a) *Uncracked* specimens, which were never loaded.
- (b) *Unloaded* specimens, which were loaded only once to induce cracking.
- (c) *Cyclic* specimens, which were subjected to five load cycles to promote greater damage at the rebar-concrete interface.
- (d) *Loaded* specimens, which were initially pre-cracked and subsequently reloaded with a sustained load to keep cracks open.

For all the beams subjected to loading, crack widths ranging from 0.1 to 0.4 mm were investigated. Moreover, four different series of specimens were cast:

- (a) *Plain* series: without fibre reinforcement.
- (b) *Steel* series: containing 0.5 % vol. of 35 mm end-hooked low-carbon steel fibres.
- (c) *Hybrid* series: combining 0.35% vol. steel fibres and 0.15% 18 mm straight PVA fibres.
- (d) *Synthetic* series: with 0.75% vol. 30 mm straight PVA fibres.

The specimens used in the experimental study were 1100 mm long beams with cross-sectional dimensions of 180×100 mm and reinforced with three Ø10 mm ribbed bars positioned with a clear concrete cover of 30 mm from the bottom and lateral sides. A self-compacting concrete mix with a water/cement ratio (w/c) of 0.47 was used for all the series in the experimental study. The reinforcement bars were of B500B steel grade and were used “as received” without applying any surface treatment prior to casting. Figure 1(a) shows the geometry of the beam specimens, including the reinforcement layout, and the different types of fibres used.

Experimental study A was subdivided into two phases. The first phase involved the pre-cracking and subsequent conditioning of the beams through cycles of partial immersion in 16.5% wt. NaCl solution beams to promote chloride-induced corrosion of the reinforcement. During the first phase, half-cell potential and corrosion rate measurements were performed periodically on two reinforcement bars from each beam, see Figure 1(b). The second phase

involved the assessment of the structural performance of the corroded RC beams and its correlation to the actual corrosion levels evaluated through weight loss measurements and 3D scanning technique. The setup used for the pre-cracking and structural assessment of the beams is illustrated in Figure 1(c) whereas an example of a 3D scanned pit and the corresponding sectional loss analysis are depicted in Figure 1(d). For further details on the experimental setup, the reader is referred to (Berrocal, 2017).

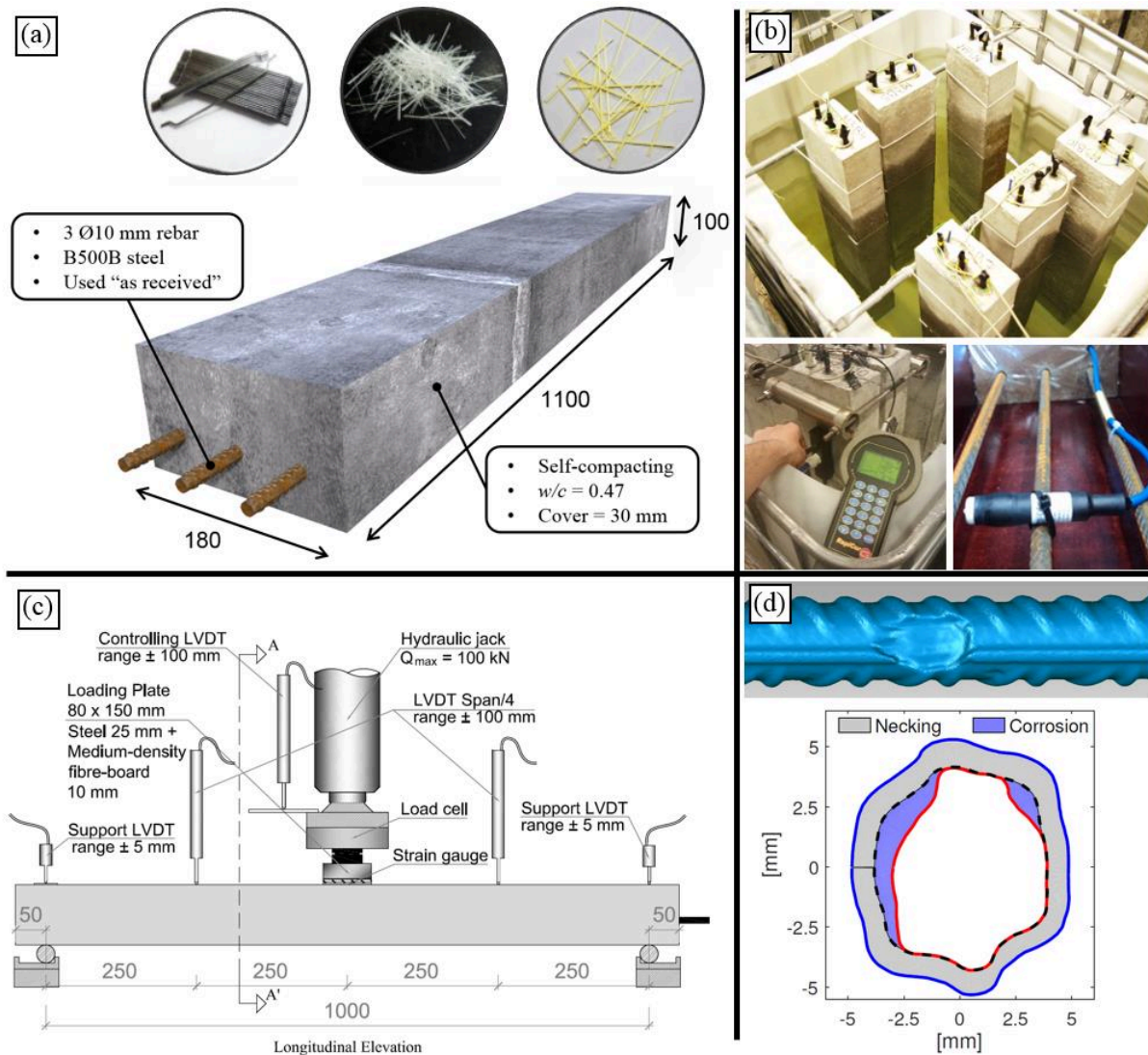


Figure 1: (a) Specimen geometry, reinforcement layout and fibre types. (b) Beams partially immersed in 16.5% wt. solution and the equipment used to monitor corrosion rate, RapiCor (left) and half-cell potential, ERE 20 (right). (c) Three-point bending setup used to pre-crack and assess the structural performance of the beams. (d) 3D scanned reinforcement bar displaying a corrosion pit and results of the sectional analysis to determine the local reduction of cross-section due to necking and due to corrosion. Measurements in mm.

2.2 Experimental study B: internal crack morphology

Three different concrete mixes were used to cast a total of twelve beams: plain concrete (PC) and steel fibre reinforced concrete (SFRC) as previously described, and a modified hybrid reinforced concrete (HyFRC) mix combining 35 mm long steel macro fibres at 0.5%